

A Torque-Actuated Dissipative Spring Loaded Inverted Pendulum Model with Rolling Contact and its use as the Template for Design and Dynamic Behavior Generation on a Hexapod Robot

Chia-Jui Hu, Chun-Kai Huang, and Pei-Chun Lin

Abstract- We report on a model-based approach for robot design and its dynamic motion generation. A new torque-actuated dissipative spring loaded inverted pendulum model with rolling contact (TDR-SLIP) is proposed to serve as the motion template for the robot. It is a successor to a previously developed spring loaded inverted pendulum model with rolling contact (R-SLIP) model but with embedded energy flow, which has better mapping to empirical robots. The stability properties of the TDR-SLIP model are analyzed, and its stable motion trajectory is implemented on the robot as the control guidance. The robot leg is developed according to the morphology and function of the TDR-SLIP leg, which acts as the design guidance. The proposed model-based approach is experimentally evaluated and finds that the robot is able to exhibit running behavior with various speeds and leg mechanics settings.

I. INTRODUCTION

Legged animals have great ability in negotiating rough terrain. It has long been asked how animals evolved leg morphology and how these legs are coordinated for agile locomotion, but answers are still limited. On the modeling side, one approach to addressing this issue is to search for adequate motion models to represent animals' locomotion. More specifically, reduced-order models are generally adopted not only because they are simpler and easier to deal with, but also because the simpler model can preserve the essential characteristics of legged locomotion while ignoring the complexity of some other minor effects. Thus, the applicable domain of the model can be extended to its largest range. On the robotics side, various robots are built based on certain biological inspirations or design philosophies, and their dynamic performances are usually compared and evaluated according to those of the reduced-order models.

In the past few decades, various models and legged robots have been reported and analyzed. Among all the reduced-order models, the Spring Loaded Inverse Pendulum (SLIP) is the most well-known [1, 2]. Simply composed of a point mass and a massless linear spring, the SLIP model successfully captures the characteristics of the center-of-mass (CoM) motion of multi-legged animals, thus serving as the fundamental "template" for legged locomotion [3]. Later, several other models based on the SLIP were reported, each addressing some real-world issues in order to develop the

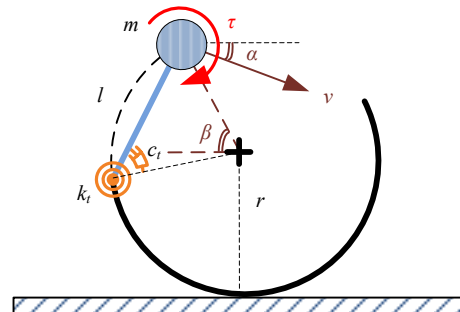


Fig. 1. Six parameters and three initial conditions of the TDR-SLIP model.

models to better fit reality. Some examples of these models include one with two-segment legs [4], one with a rolling foot [5], one with clocked torque [6] or constant torque [7] and damping terms, etc. On the robotics side, the Sprawl series [8], RHex series [9], Scout series [10], and Tekken series [11] are a few examples of robots that are able to perform dynamic behaviors. Some of them are loosely based on the SLIP model, and some of the built robots are specifically tuned to exhibit the SLIP model. However, none of the robots are specifically and tightly designed based on the reduced-order model. To the best of our knowledge, the only robot which approaches this protocol is the dynamic climbing robot [12].

Previously, we successfully used the Rolling-SLIP (R-SLIP) model as the "template" to exhibit dynamic running behavior in the RHex-style robot – the "anchor" [13]. The morphology and mechanism of the model was inspired by the solid mechanics of the compliant half-circular legs of the robot, thus better capturing its nature dynamics. By matching the operation point of the robot to that of the stable fixed-point motion of the R-SLIP model, the robot could easily perform dynamic running at various speeds without any tuning or optimization effort. However, the energy conservative characteristics of the R-SLIP model also prevented the "template-anchor" mapping from the model onto the empirical robot at the deeper level. More specifically, the usual control input of the robot – the motor torque – had no obvious link to the behavior of the robot.

This work is supported by National Taiwan University (NTU) under contract NTU-CDP-102R7817 and the National Science Council (NSC), Taiwan under contract NSC 102-2221-E-002 -214 -MY3.

Authors are with the Department of Mechanical Engineering, National Taiwan University (NTU), No.1 Roosevelt Rd. Sec.4, Taipei, Taiwan. (Corresponding email: peichunlin@ntu.edu.tw).

Here, aiming to investigate the design and control relationship between the reduced-order model (i.e. the “template”) and the empirical robot (i.e. the “anchor”), we report on (i) the development of a new reduced-order model, the torque-actuated dissipative SLIP model with rolling contact (TDR-SLIP) as shown in Fig. 1. It is the successor of the R-SLIP model which had torque and damping terms. (ii) The new robot (mainly leg) design based on this new model. As a result, there is a clear “template-anchor” relationship and the dynamic behavior of the robot can ideally be excited by using the model.

The rest of the article is divided into four sections. Section II introduces the TDR-SLIP model. Section III shows the model-based robot design, with emphasis on the leg design. Section IV describes the experiment results, and Section V concludes the work.

II. CHARACTERISTICS OF THE TDR-SLIP MODEL

The TDR-SLIP model is composed of a point mass, two massless segments connected by a revolute joint, a rotary and parallel-installed spring-damper system mounted on the joint, and torque acting on the upper segment with an axis passing the mass as shown in Fig. 1(a). The lower segment has a circular shape which rolls on the ground without sliding. The mass is mounted on the opposite end of the upper segment. The model has elastic and energy-dissipative properties, and will serve as the template for the legged robot with half-circular legs. The TDR-SLIP has six intrinsic parameters: mass (m), length of the upper segment (l), radius of the lower segment (r), torsional spring constant (k_t), and rotational damping constant (c_t). It also has one external input, torque (τ). Similar to the behavior of other SLIP-like dynamic models, that of the TDR-SLIP is composed of stance phase and flight phase, alternating periodically if the model runs stably. The transitions from the former to the latter and vice versa are defined as liftoff and touchdown, respectively.

The dynamic behavior of the TDR-SLIP model in stance phase can be derived by using the Lagrangian method. Two angles θ and φ are chosen as the general coordinates for the model derivation as shown in Fig. 2. The symbol θ refers to the angle formed by the horizontal line and the upper segment, and the symbol φ refers to the angle between the upper segment and the line segment connecting the revolute joint to the center of the lower segment. By this definition, the angle θ represents how the leg swings and is an active degree-of-freedom (DOF) as the torque involved, while the angle φ represents the compression level of the spring-damping system. While the model is in its stance phase, displacement of the mass in Cartesian coordinates, (x_s, y_s) , can be represented as

$$\begin{aligned} x_s &= r(\varphi - \varphi_0 - \theta + \theta_0) - r \cos(\varphi - \theta) + l \cos(\theta) \\ y_s &= r + r \sin(\varphi - \theta) + l \sin(\theta) \end{aligned} \quad (1)$$

where the subscript s indicates stance phase. Velocity of the mass can be yielded by derivation of (1)

$$\begin{aligned} \dot{x}_s &= r(1 + \sin(\varphi - \theta))(\dot{\varphi} - \dot{\theta}) - l \sin(\theta)\dot{\theta} \\ \dot{y}_s &= r \cos(\varphi - \theta)(\dot{\varphi} - \dot{\theta}) + l \cos(\theta)\dot{\theta} \end{aligned} \quad (2)$$

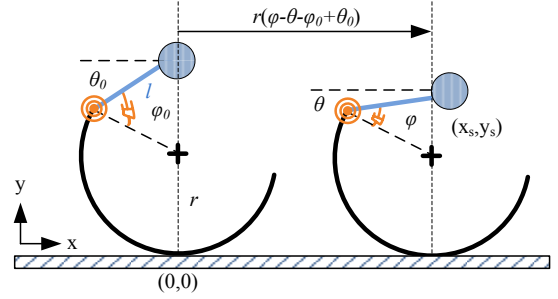


Fig. 2. Two generalized coordinates for the model development.

Then kinematic energy T and potential energy V of the model can be written as

$$T = m\{r^2[1 + \sin(\varphi - \theta)](\dot{\varphi} - \dot{\theta})^2 + rl(\cos(\varphi) - \sin(\theta))(\dot{\varphi}\dot{\theta} - \dot{\theta}^2) + \frac{1}{2}l^2\dot{\theta}^2\} \quad (3)$$

and

$$V = \frac{1}{2}k_t(\varphi_0 - \varphi)^2 + mg(r + r\sin(\varphi - \theta) + l\sin(\theta)), \quad (4)$$

respectively. Because the TDR-SLIP model incorporates a damper which means it is not energy-conservative, the Rayleigh dissipation function is included in the Lagrange equation

$$F = \frac{1}{2}c_t\dot{\varphi}^2. \quad (5)$$

To remedy the energy loss of the model during motion, external torque is applied to the upper segment with the axis passing the mass (i.e. the same position as the generalized coordinate θ is defined)

$$\begin{aligned} Q(\theta) &= \tau \\ Q(\varphi) &= 0 \end{aligned} \quad (6)$$

With the energy input from the torque, the model can maintain roughly the same level of energy to enable stable and periodic locomotion. Following that, the dynamic equations with respect to two generalized coordinates can be written as

$$\begin{cases} \frac{d}{dt} \left(\frac{\partial L}{\partial \dot{\theta}_i} \right) - \frac{\partial L}{\partial \theta_i} + \frac{\partial F}{\partial \dot{\theta}_i} = \tau \\ \frac{d}{dt} \left(\frac{\partial L}{\partial \dot{\varphi}_i} \right) - \frac{\partial L}{\partial \varphi_i} + \frac{\partial F}{\partial \dot{\varphi}_i} = 0 \end{cases} \quad (7)$$

By importing (3)-(6) into (7), the quantitative representations of the equations of motion can be expressed as

$$\begin{aligned} &ml^2 - 2mrl(\cos\varphi - \sin\theta) + 2mr^2(1 + \sin(\varphi - \theta))\ddot{\theta} \\ &+ mrl(\cos\varphi - \sin\theta) - 2mr^2(1 + \sin(\varphi - \theta))\ddot{\varphi} \\ &- mr^2(\dot{\varphi} - \dot{\theta})^2 \cos(\varphi - \theta) - mrl(\dot{\varphi}^2 - 2\dot{\varphi}\dot{\theta})\sin\varphi \\ &+ mrl\dot{\theta}^2 \cos\theta + mg(l\cos\theta - r\cos(\varphi - \theta)) = \tau \\ &mrl(\cos\varphi - \sin\theta) - 2mr^2(1 + \sin(\varphi - \theta))\ddot{\theta} \\ &+ 2mr^2(1 + \sin(\varphi - \theta))\ddot{\varphi} + mr^2(\dot{\varphi} - \dot{\theta})^2 \cos(\varphi - \theta) \\ &- mrl\dot{\theta}^2(\cos\theta + \sin\varphi) + mgr\cos(\varphi - \theta) + k_t(\varphi - \varphi_0) \\ &+ c_t\dot{\varphi} = 0 \end{aligned} \quad (8)$$

Together with the initial conditions (ICs), the dynamic behavior of the TDR-SLIP model in its stance phase can be numerically simulated. The ICs of the model are usually given at the moment of touchdown (i.e. beginning of the stance phase), which includes the landing angle (β), touchdown speed (v), and touchdown angle formed by the touchdown

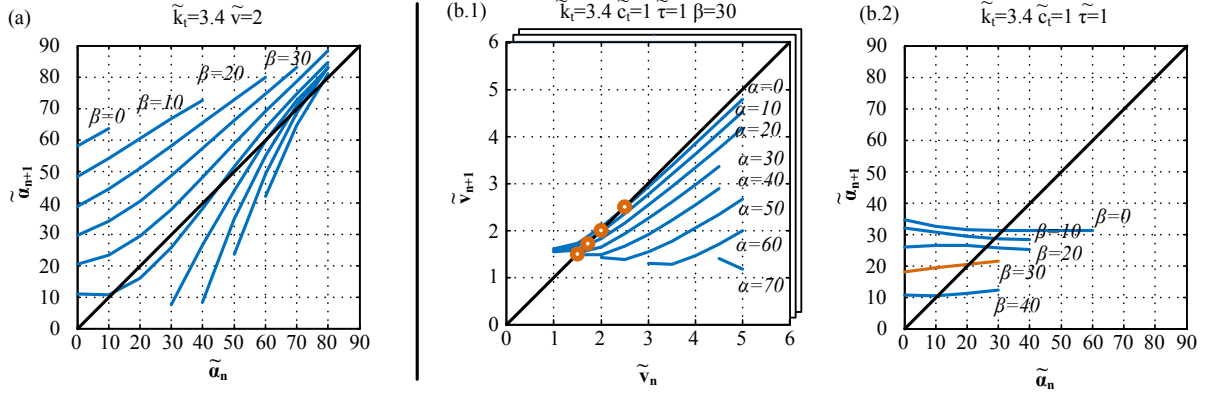


Fig. 3. Stability analysis of the TDR-SLIP model: (a) The one-dimension return map; (b) The process of finding fixed points with two-dimension return map: (b.1) Constructing the return map of touchdown speed v of the model with a fixed landing angle and various touchdown angles, and (b.2) constructing the return map of touchdown angle α of the model with various landing angles. The orange points in (b.1) are equivalent to the orange curve in (b.2). This analysis process is repeated several times using different landing angles.

velocity and the horizontal line (α) as shown in Fig. 1(a). On the other hand, the dynamic behavior of the model in its flight phase is merely a ballistic flight affected by gravity only, so the equations of motion can be expressed as

$$\begin{aligned} x_f &= x_{LO} + \dot{x}_{LO}t \\ y_f &= y_{LO} + \dot{y}_{LO}t - \frac{1}{2}gt^2, \end{aligned} \quad (9)$$

where the symbols g , f , and LO indicate the gravity constant, flight phase, and liftoff moment, respectively.

Transition of the model from flight phase to stance phase (i.e. touchdown) or vice versa (i.e. liftoff) takes place under certain conditions. Touchdown of the model occurs when mass height decreases during its ballistic flight and reaches the geometric relationship

$$y_{TD} = r + r\sin(\beta), \quad (10)$$

where the symbol TD indicates the touchdown moment. On the other hand, liftoff of the model occurs when the vertical ground-reaction force is equal to gravity. In addition, the following two conditions are necessary to ensure continuous running of the model. First, at liftoff, the horizontal velocity of the mass should be positive for continuing forward motion $\dot{x}_{LO} > 0$.

Second, the mass height of the model at liftoff needs to be high enough for successful touchdown for the next stance phase

$$y_{LO} + \frac{\dot{y}_{LO}^2}{2g} > r + r\sin(\beta). \quad (12)$$

Note that in reality, when the leg with mass touches down on the ground, the leg suffers an impact force which dramatically changes its momentum almost immediately. During this process, some energy dissipates in the form of heat, sound, and deformation. In our setting, as with other developments of the reduced-order models, the leg is massless and therefore the energy-consuming impact is absent from the model. The point mass above the spring does not suffer impact either; this is because the spring acts as a medium for smooth energy transition. As a result, the damper on the leg is the only energy dissipative source. In addition, all the analysis work is done in a dimensionless manner, and the variables of TDR-SLIP include $\tilde{\tau} = \frac{\tau}{mgl_0}$, $\tilde{k}_t = \frac{k_t}{mgl_0}$, $\tilde{c}_t = \frac{c_t}{ml_0\sqrt{gl_0}}$, $\tilde{v} = \frac{v}{\sqrt{gl_0}}$, $\tilde{\alpha} = \alpha$, and $\tilde{\beta} = \beta$.

Finding fixed points is a typical method for analyzing the stability characteristics of the model. This is generally facilitated by using a return map analysis. For ordinary energy-conservative systems, the search for fixed points is one dimensional, and this indicates that the system can be regarded as stable as long as one of the state variables of the system, x , remains unchanged throughout the motion (i.e. satisfying $x_{n+1} = x_n = x^*$). However, because the proposed TDR-SLIP model is not energy conservative, even when one of the states reaches its equilibrium (for example, touchdown angle α with $\alpha_{n+1} = \alpha_n = \alpha^*$), the model may not repeat its original motion but may gradually deviate to some other status. Thus, the two-dimensional map is essential, as reported in [7, 14]. In addition to the touchdown angle, the touchdown speed is chosen for analysis with criterion $v_{n+1} = v_n = v^*$, and this criterion is introduced to equalize the energy level in the model. The solving procedure is briefly described as follows. First, investigate the return map of the touchdown speed with a specific landing and different touchdown angles, as shown in Fig 3(b.1), where each line represents the model with a specific touchdown angle. Second, extract the fixed points plotted on the figure (i.e. intersecting with the black diagonal line), and replot them on the return map of the touchdown angle, forming a line segment. Third, repeat steps one and two with different landing angles, and the final plot consists of several lines as shown in Fig. 3(b.2), where each line represents the model with a specific landing angle. Finally, extract the fixed points plotted on the figure, which are the points satisfying the stability criterion.

After the fixed points are determined, the next task is to check whether they are stable or not. Because the entire motion in stance phase cannot be integrated, it is difficult to find the exact Jacobian matrix for stability analysis. Therefore, we adopted the method reported in [7], where eigenvalues for an approximate numerical Jacobian matrix are utilized to determine the model's stability.

$$J = \begin{bmatrix} (\tilde{v}_{\Delta v}^{next} - \tilde{v}^*)/\Delta v & (\tilde{v}_{\Delta \alpha}^{next} - \tilde{v}^*)/\Delta \alpha \\ (\alpha_{\Delta v}^{next} - \alpha^*)/\Delta v & (\alpha_{\Delta \alpha}^{next} - \alpha^*)/\Delta \alpha \end{bmatrix} \quad (13)$$

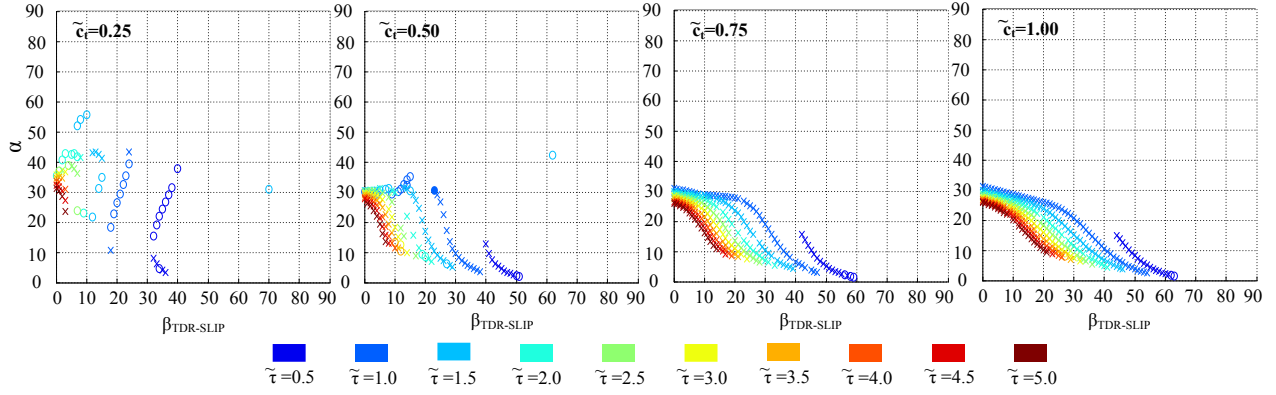


Fig. 5. Locations of fixed points of the TDR-SLIP model. Dots with different colors represent different torque values. Different rows represent different dimensionless damping constants, varying from 0.25 to 1.

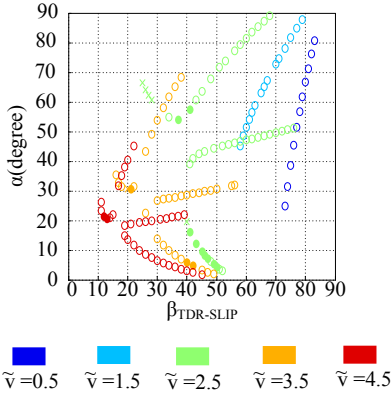


Fig. 4. Locations of fixed points of the R-SLIP model. Dots with different colors represent different velocity values.

In each evaluation, a 1% disturbance is given to one variable and the state variation is checked after one-period motion. Next, the matrix shown in (13) can be numerically determined, and this corresponding Jacobian matrix is utilized to check the convergence property from stride to stride. If any eigenvalue of (13) has a magnitude greater than 1, the fixed point is unstable. If both eigenvalues have a magnitude of less than 1, the fixed point is asymptotically stable. If one of the eigenvalues has a magnitude equal to 1 and the other eigenvalue has a magnitude of less than 1, the fixed point is marginally stable.

Figure 4 shows the locations of fixed points of the R-SLIP model. Different colors represent the model with different dimensionless velocities, and the symbols \circ , \bullet , and \times represent unstable, marginally stable, and asymptotically stable fixed points, respectively. Figure 5 then shows the locations of the fixed points of both the TDR-SLIP model with different parameter settings and the ICs. Different colors represent the model with different dimensionless torques. We also find several facts from Fig. 5. (i) As the damping constant increases, the number of stable fixed points increases and the existence area of fixed points become larger in the direction of the landing angle. In the robotic application, the landing angle is usually directly controllable (i.e. by joint motors). Thus, the TDR-SLIP model with a higher damping constant, which allows a wider range of landing angles, is more flexible. (ii) The fixed points of the TDR-SLIP model exist with small

touchdown angles and landing angles. At the same time, many fixed points of the R-SLIP model exist with large touchdown angles and landing angles. Therefore, the TDR-SLIP does not have the jumping gait of the R-SLIP model, but uses all of its energy in forward running. (iii) The locations of the fixed points of the TDR-SLIP model with different torques are closely spaced, which indicates that the torque can be controlled in a non-strict manner. When the torque is not applied at the right value, the performance of the model remains similar since the correct ICs of the given torque locate nearby. (iv) As reported in the literature and observed in the TDR-SLIP model, the torque and damper of the model should be matched to allow stable running. Figure 5 reveals that as the damping constant increases, the number of stable fixed points increases with the increase of torque. This observation is intuitively correct since the torque is an energy input, so if the damping constant is small, the energy cannot dissipate appropriately.

III. ROBOT DESIGN

The model-based robot design process mainly relies on the leg morphology and function. Previously, we completed the “template and anchor” experiment using the R-SLIP model on a RHex-style robot. RHex is a hexapod robot that originated at the University of Michigan. It has only one active rotational DOF per leg, each of which is made with compliant materials mimicking the elastic behavior of running animals. In that work, mapping was constructed between the complex half-circular compliant leg and the 1-DOF reduced-order leg. In this current robot, while the general morphology of the body remains the same (i.e. rigid body, hexapod morphology, one active rotational DOF per leg) as shown in Fig. 6(a), the robot leg is completely redesigned to match the morphology and function of the TDR-SLIP model leg. Thus, the leg has an identical shape to the TDR-SLIP leg, and has rotational spring and damper components.

The unique curved leg shown in Fig 7(a) is designed for the realization of the TDR-SLIP model leg. The leg, like the model, is made up of two parts: the upper beam and the lower rim. The parallel dynamic system, composed of a torsion spring and damper, connects the upper and lower structures. The spring constant is chosen according to the optimal variable table from our previous research [13]. The damping

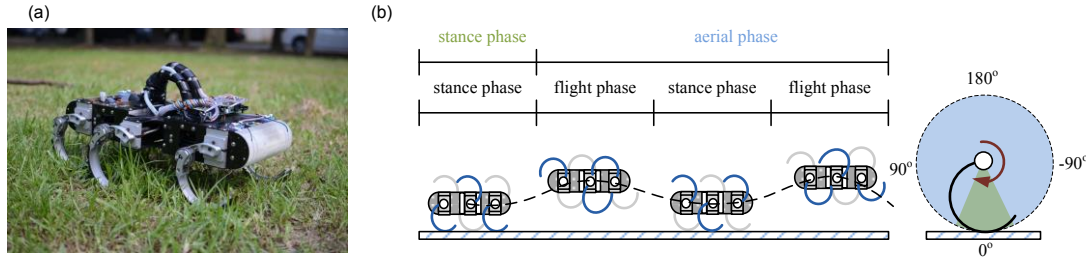


Fig. 6. The robot and its motion generation: (a) the RHex-style robot with TDR-LSIP legs; (b) The mapping from the TDR-SLIP motion to the robot

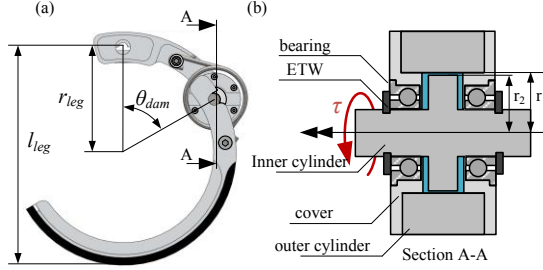


Fig. 7. Realization of the TDR-SLIP leg: (a) Leg configuration; (b) The cross section of the damper. The blue area is the oil chamber.

TABLE I THE SPECIFICATION OF THE LEG

| | |
|-------------------|-------|
| weight | 260g |
| Damper position | 60° |
| Curved radius | 70mm |
| Width (Curve leg) | 30mm |
| Width (bar) | 18mm |
| Leg length | 146mm |

TABLE II THE PROPERTIES OF THE SILICON OILS

| Kinematic Viscosity mm ² /s | 200,000 | 500,000 | 1000,000 |
|--|---------|---------|----------|
| w | 64.88 | 62.07 | 62.831 |
| c _i /2I | 21 | 28.5 | 47.2 |
| c _i /k _i | 0.0099 | 0.0148 | 0.0239 |
| Design c _t | 0.07 | 0.09 | 0.17 |
| c _t | 0.069 | 0.1036 | 0.1674 |
| error | 0.5% | 15% | 1.5% |

coefficient is chosen from the existing spring damping ratio in [15] with its several multiples. The damper is designed by using the principle of a coaxial rotating cylinder viscometer [16, 17]. The detailed components of the damper box are shown in Fig 7(b); this mechanism comprises covers, an inner cylinder and an outer cylinder. The chamber of the damper is designed to be filled with the high viscosity fluid.

The design is based on several assumptions: (i) the liquid is incompressible; (ii) the motion is laminar; (iii) the stream lines of the liquid are circular; (iv) the speed is a function of radius only and there are no other velocity changes in axis direction; (v) there is no slip between the liquid and the cylinder. Then, the velocity change in the radial direction can be represented as

$$\frac{dv}{dr} = \omega + r \frac{d\omega}{dr} \quad (23)$$

The ω term in (23) is generated by the radius difference, so it is not taken into consideration for the viscosity problem. By putting (23) into the definition of the viscosity we obtain the relationship between the viscosity constant and the torque

$$\eta = \frac{F}{A \frac{dv}{dy}} = \frac{F}{rA \frac{d\omega}{dr}} = \frac{\tau/r}{rA \frac{d\omega}{dr}} = \frac{\tau}{2\pi l r^3 d\omega} \quad (24)$$

By integral equation (24), we get

$$\omega_{r_1} - \omega_{r_2} = \frac{\tau}{4\pi l \eta} \left(\frac{1}{r_1^2} - \frac{1}{r_2^2} \right) \quad (25)$$

As a result, the rotational damping constant can be written as

$$c_t = \frac{\tau}{\Delta\omega} = \frac{4\pi l \eta}{\left(\frac{1}{r_2^2} - \frac{1}{r_1^2} \right)} \quad (26)$$

Silicon oil is used in our damper box for its stability and wide range of viscosities. The other geometric dimensions are restricted by the size of the leg of our previous robot version [18] in order to maintain interchangeability. The leg data is recorded in Table I.

The properties of the damper are determined by the free vibration method. By watching the decay constant and the vibration frequency of the spring-damper parallel system, the damping coefficient can be found by solving the ordinary differential equation (ODE). The final result is lower than the design value – about 20% of the expected number. The shape of the inner and outer cylinder is then redesigned to increase the contact surface to compensate the loss caused by the high speed. The final damping coefficient of the damper box is 0.17, which is 60% of our initial goal. This is the largest damping coefficient that can be achieved given the fabrication and dimension constraints of the machining process. The final results are listed in Table II.

With the newly designed legs, the robot motion is generated following the strategy previously adopted. The widely-used alternating tripod gait is adopted for these running experiments owing to its stable and fast locomotion. The tripod legs provide stable motion for the spatial rigid robot motion (i.e. less pitch and roll). In addition, the two tripods are programmed to move in an alternating and symmetric manner; thus the robot should ideally move straight ahead (i.e. with less lateral displacement and yaw motion). As a result, the motion of the four un-modeled motion DOFs of the real robot should exhibit minimal variations. Figure 6(b) shows the schematic motion sequence of the robot with a tripod gait and the TDR-SLIP model. Because the robot is set to move as per the TDR-SLIP model, a full stride should include a stance phase and flight phase. In order to let the CoM move according to the TDR-SLIP model in the stance phase, all three legs of the tripod are synchronically actuated and rotated according to the TDR-SLIP trajectory while they roll on the ground. Based on the assumption that the robot body remains horizontal during the whole of the stance phase, the leg orientation with respect to

the body is actually equal to the generalized coordinate θ of the TDR-SLIP model. On the other hand, the period of the leg's flight phase is much longer than that of the R-SLIP model because the two tripod legs are alternating. The flight phase of the leg covers two flight phases and one stance phase of the TDR-SLIP model as shown in Fig. 6(b).

IV. EXPERIMENT

The strategy of model-based robot design and motion generation is experimentally evaluated. In the experiment we choose legs with silicon oil with a viscosity of 500,000 mm²/s and 1000,000 mm²/s in order to realize the TDR-SLIP model; we use legs without oil to realize the R-SLIP model, for comparison. All experiment data is recorded by the ground truth measurement system (GTMS) which is composed of two 250Hz high speed cameras and two 6-axis force plates. The robot runs at two speeds: 1.5m/s and 2m/s. In order to maintain motion consistency while the robot runs with different models, the fixed points of different models are chosen to have similar ICs. Figure 8 plots the robot's experiment results. The plot clearly shows that the forces in the fore/aft and vertical directions, F_x and F_z , are zero for about 35-40% of each period, indicating the robot in flight phase. This confirms that the robot is operating in the dynamic running motion. The figure also shows that some delay exists for the model state change. This phenomenon is mainly caused by the fact that the spring-damper parallel system on the leg is still in compression when the robot starts to jump. The recovery force of the parallel system acts on the force plates, causing the ground-reacting forces to exhibit some delay in returning to zero. The experimental result is quite comparable to the trajectory of the vertical velocity of the model. In contrast, the forward velocity exhibits some offset, owing to slipping on the ground. TDR-SLIP needs a larger friction force to maintain the counter-torque of the motor than R-SLIP does, which accounts for the larger speed difference in TDR-SLIP versus the R-SLIP. In terms of the force, the experimental results exhibit a single compression in the vertical direction and a deceleration/acceleration pattern in the fore/aft direction – a typical running motion pattern. In the meantime, there exists a certain difference between the model setting and the robot behavior. In the simulation, torque is built instantly when the TDR-SLIP model touches the ground, yielding the nonzero forces during leg touchdown. In contrast, the ground-reaction forces of the empirical robot rise gradually after the leg touches the ground. Though not perfect, the TDR-SLIP method has certain advantages over the R-SLIP. First, the passive running trajectory in the TDR-SLIP model does not have “reverse” leg rotation as it does in the R-SLIP model. Reverse rotation would require the empirical motor to have high power and a fast response. Second, the robot running with the TDR-SLIP model is more stable as it has less standard deviation of motion. The high motion repeatability means that the TDR-SLIP can better reject disturbances from the environment. At the same time, as shown in Fig. 9, the TDR-SLIP model successfully suppresses the body pitch vibration, indicating that the torque and damper indeed have a positive influence on the dynamic behavior of the robot.

V. CONCLUSION

We report on the development and evaluation of the model-based robot design and control strategy. Aimed at extending the previously developed R-SLIP model with realistic energy flow setup, the TDR-SLIP model is developed to serve as the template for the robot design. The stability properties of the models were analyzed numerically via return map analysis and several conclusions can be drawn. (i) The number of fixed points increases with the increase of torque and damping constants. (ii) By using the approximated Jacobian matrix for stability analysis, some fixed points are recognized as stable fixed points. (iii) The number of stable fixed points in the TDR-SLIP model is larger than that of the R-SLIP model. (iv) The TDR-SLIP can tolerate a wider range of torque variation. After the analysis, some of the stable trajectories of the TDR-SLIP model are selected for implementation on the robot as the control guidance.

On the design side, the robot leg is designed to match the morphology and function of the TDR-SLIP leg. The damping property of the leg can be altered by changing the viscosity of the silicon oil inside the damper. The free vibration experiment confirms that the function is effective, but that the quantitative effect is less than the estimation derived from the simple viscosity model.

The robot running experiments are executed to evaluate the effectiveness of the model-based robot design and control approach. The results confirm that the robot can perform the running behavior at two designed speeds and with three leg-property settings. Owing to the constant torque setting, the robot running with the TDR-SLIP model has more ground slippage than with the R-SLIP. Yet it has several advantages over the R-SLIP model: pitch disturbance rejection and running motion repeatability, which simultaneously reduce the motor power requirement.

We are currently modifying the input torque profile so that the model condition can be better matched to real conditions. In the meantime, we are exploring other dynamic gaits on the robot to deepen the usage of the TDR-SLIP model as a template.

VI. REFERENCES

- [1] R. Blickhan, "The spring mass model for running and hopping," *Journal of Biomechanics*, vol. 22, pp. 1217-1227, 1989.
- [2] T. A. McMahon, "Elastic mechanisms in animal movement - Alexander, R.M.," *Nature*, vol. 336, pp. 530-530, Dec 1988.
- [3] R. J. Full and D. E. Koditschek, "Templates and anchors: Neuromechanical hypotheses of legged locomotion on land," *Journal of Experimental Biology*, vol. 202, pp. 3325-3332, Dec 1999.
- [4] J. Rummel and A. Seyfarth, "Stable running with segmented legs," *International Journal of Robotics Research*, vol. 27, pp. 919-934, Aug 2008.
- [5] J. Y. Jun and J. E. Clark, "Effect of rolling on running performance," in *IEEE International Conference on Robotics and Automation (ICRA)*, 2011, pp. 2009-2014.
- [6] J. Seipel and P. Holmes, "A simple model for clock-actuated legged locomotion," *Regular & Chaotic Dynamics*, vol. 12, pp. 502-520, Oct 2007.
- [7] Z. Shen and J. Seipel, "A fundamental mechanism of legged locomotion with hip torque and leg damping," *Bioinspiration & Biomimetics*, vol. 7, p. 046010, 2012.
- [8] J. G. Cham, S. A. Bailey, J. E. Clark, R. J. Full, and M. R. Cutkosky, "Fast and robust: Hexapedal robots via shape deposition manufacturing,"

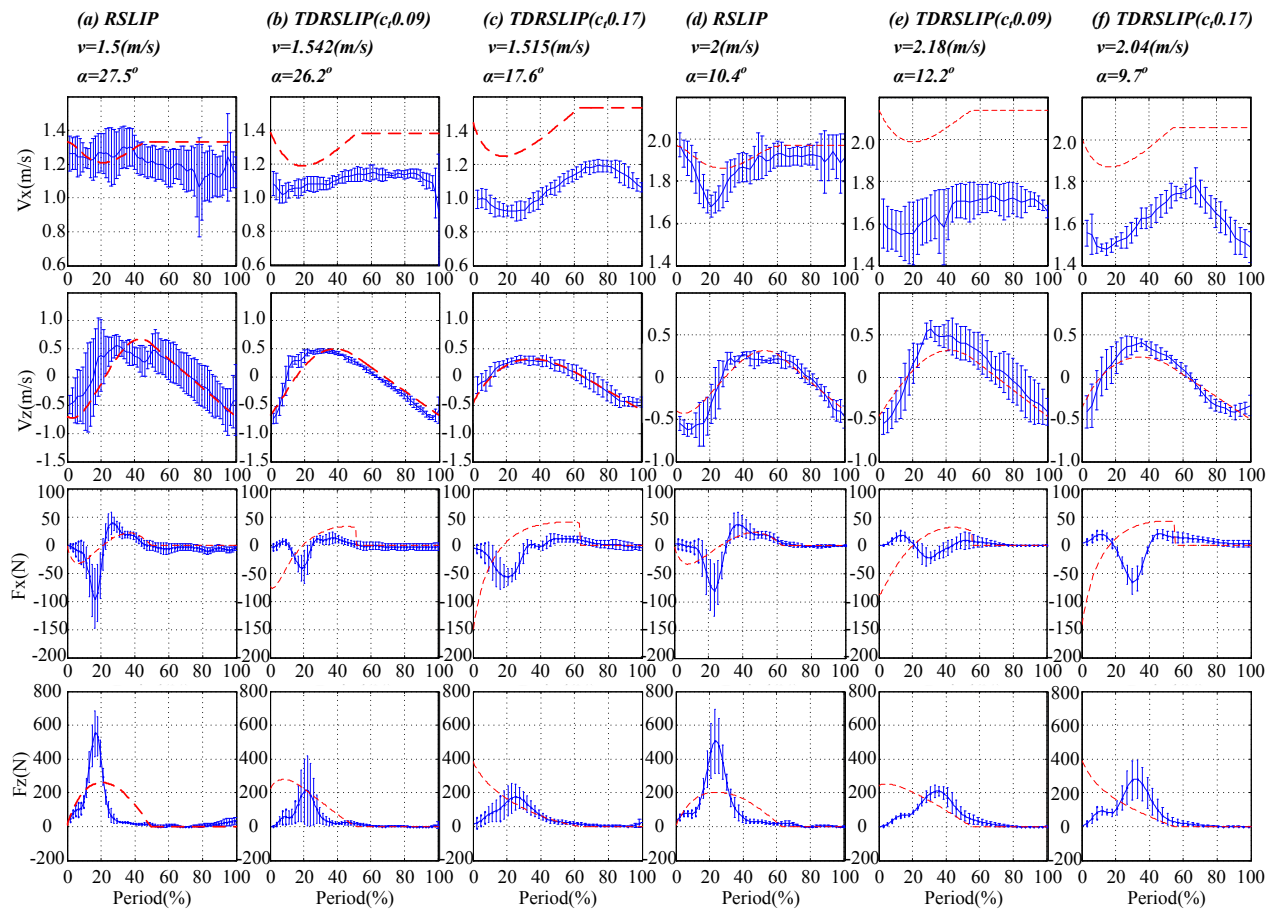


Fig. 8. The experimental data of robot running measured by the GTMS. The four columns from left to right are velocity and ground reaction forces in the fore/aft and vertical directions (V_x , V_z , F_x , and F_z), respectively. The first three and last three rows are the data with the robot running at 1.5m/s and 2m/s, accordingly. In each set, the columns from the top to the bottom are for the robot running with the R-SLIP model, the TDR-SLIP model with moderately sticky damper, and the TDR-SLIP model with very sticky damper. The red dashed curves are from the TDR-SLIP model, and the blue curves and vertical bars are the mean and standard deviations of five experimental runs.

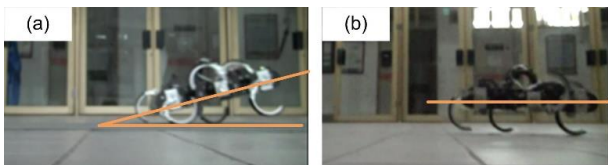


Fig. 9. The robot running with (a) the R-SLIP model and (b) the TDR-SLIP model. The former has a larger pitch vibration than the latter.

The International Journal of Robotics Research, vol. 21, pp. 869-882, 2002.

- [9] U. Saranli, M. Buehler, and D. E. Koditschek, "RHex: A simple and highly mobile hexapod robot," *International Journal of Robotics Research*, vol. 20, pp. 616-631, Jul 2001.
- [10] I. Poulakakis, J. A. Smith, and M. Buehler, "Modeling and experiments of untethered quadrupedal running with a bounding gait: The Scout II robot," *The International Journal of Robotics Research*, vol. 24, pp. 239-256, 2005.
- [11] H. Kimura, Y. Fukuoka, and A. H. Cohen, "Adaptive dynamic walking of a quadruped robot on natural ground based on biological concepts," *International Journal of Robotics Research*, vol. 26, pp. 475-490, May 2007.
- [12] G. A. Lynch, J. E. Clark, P. C. Lin, and D. E. Koditschek, "A Bioinspired Dynamical Vertical Climbing Robot," *International Journal of Robotic Research* vol. 31, pp. 974-996, 2012.
- [13] K. J. Huang, C. K. Huang, and P. C. Lin, "A Simple Running Model with Rolling Contact and Its Role as a Template for Dynamic Locomotion on a Hexapod Robot," *Bioinspiration & Biomimetics*, vol. 9, p. 046004 (20pp), 2014.
- [14] M. M. Ankarali and U. Saranli, "Stride-to-stride energy regulation for robust self-stability of a torque-actuated dissipative spring-mass hopper," *Chaos*, vol. 20, p. 033121, Sep 2010.
- [15] J. Y. Jun, "Characterization and optimization of running with curved legs," Ph.D. Dissertation, Department of Mechanical Engineering, The Florida State University, 2011.
- [16] G. Zak, A. Chan, C. Park, and B. Benhabib, "Viscosity analysis of photopolymer and glass-fibre composites for rapid layered manufacturing," *Rapid Prototyping Journal*, vol. 2, pp. 16-23, 1996.
- [17] D. Bradley, K. Zaman Dahlan, and S. Roy, "Measurement of the viscosity of irradiated silicone using a differential viscometer," *Applied Radiation and Isotopes*, vol. 53, pp. 921-928, 2000.
- [18] Y. C. Chou, W. S. Yu, K. J. Huang, and P. C. Lin, "Bio-inspired step-climbing in a hexapod robot," *Bioinspiration & Biomimetics*, vol. 7, p. 036008 (19pp), 2012.